Check for updates

Enhanced sorption in an indium-acetylenedicarboxylate metal–organic framework with unexpected chains of *cis*-μ-OH-connected {InO$_6$} octahedra†

Dennis Woschko, [ID] Süheyla Yilmaz, Christian Jansen, Alex Spieß, Robert Oestreich, Tobie J. Matemb Ma Ntep [ID] and Christoph Janiak [ID] *

Single crystals of the new metal–organic framework (MOF) In-adc (HHUD-4) were obtained through the reaction of linear acetylenedicarboxylic acid (H$_2$adc) with In(NO$_3$)$_3$·xH$_2$O as a racemic conglomerate in the chiral tetragonal space groups $P4_3$22 and $P4_1$22. Fundamentally different from other MOFs with linear linkers and *trans*-μ-OH-connected infinite {MO$_6$} secondary building units as in the MIL-53-type, the linear adc^{2-} linker leads to the formation of *cis*-μ-OH connected {InO$_6$} polyhedra, which have otherwise only been found before for V-shaped ligands, as in CAU-10-H. A far-reaching implication of this finding is the possibility that *trans*-μ-OH/straight MIL-53-type MOFs will have polymorphs of CAU-10-H *cis*-μ-OH/ helical topology and *vice versa*. HHUD-4 is a microporous MOF with a BET surface area of up to 940 m^2 g^{-1} and a micropore volume of up to 0.39 cm^3 g^{-1}. Additionally, HHUD-4 features good adsorption uptakes of 3.77 mmol g^{-1} for CO$_2$ and 1.25 mmol g^{-1} for CH$_4$ at 273 K and 1 bar, respectively, and a high isosteric heat of adsorption of 11.4 kJ mol^{-1} for H$_2$ with a maximum uptake of 6.36 mmol g^{-1} at 77 K and 1 bar. Vapor sorption experiments for water and volatile organic compounds (VOCs) such as benzene, cyclohexane and *n*-hexane yielded uptake values of 135, 269, 116 and 205 mg g^{-1}, respectively, at 293 K. While HHUD-4 showed unremarkable results for water uptake and low stability for water, it exhibited good stability with steep VOC uptake steps at low relative pressures and a high selectivity of 17 for benzene/cyclohexane mixtures.

Introduction

Metal–organic frameworks (MOFs) are coordination compounds consisting of metal centers or metal clusters and bridging multifunctional organic molecules, also known as linkers with a wide structural variety.[1–3] In recent years the use of acetylenedicarboxylate (adc) as a linker for MOF synthesis has attracted attention due to its high hydrophilicity, high CO$_2$ adsorption capacity and enthalpy, and the uptake of halogen vapors by the first adc-based microporous MOFs with Ce(ɪᴠ), Hf(ɪᴠ) and Zr(ɪᴠ).[4–7]

H$_2$adc is the simplest and shortest straight linear alkyne-functionalized linker, but despite its simplicity it has only recently been used in the synthesis of MOFs with proven porosity. The reason can be attributed to the low thermal stability of the H$_2$adc linker, which did not allow the synthesis of MOFs *via* hydrothermal or solvothermal methods.[8] There have been several non-porous 3D coordination networks with the adc linker being synthesized which were termed MOFs. An anionic interpenetrated [Zn(adc)$_2$]$^{2-}$ network filled with charge compensating triethylammonium ions, termed MOF-31, was achieved through a room temperature synthesis with Zn(NO$_3$)$_2$·6H$_2$O, H$_2$adc and triethylamine by Kim *et al.*[9] The 3D networks [RE$_2$(adc)$_3$(H$_2$O)$_6$] (RE^{3+} = La, Ce, Pr, Nd, Sm, Eu, Tb and Dy) by Michaelides *et al.*,[10] and Gramm *et al.*[11] or a MOF-5-analogous [Zn$_4$(O)(adc)$_3$], called IRMOF-0, by Tranchemontagne *et al.*[12] were reported as MOFs. However none of these 3D networks exhibited permanent measurable porosity, although it is noteworthy that the removal of the non-coordinating water molecules with the retention of the initial crystal structure for [Ce$_2$(adc)$_3$(H$_2$O)$_6$] was possible.[10] More successfully, H$_2$adc has been used in the synthesis of 1D to 3D coordination polymers and networks (CPs) in the work

Institut für Anorganische Chemie und Strukturchemie, Heinrich-Heine-Universität Düsseldorf, D-40204 Düsseldorf, Germany. E-mail: janiak@uni-duesseldorf.de

Paper

pioneered by the group of Ruschewitz.[4] Despite the less thermally stable H_2adc molecule the 3D networks [Sr(adc)] and [Eu(adc)] show remarkably high thermal stabilities of above 400 °C and negative thermal volume expansion.[13,14]

In 2018, the first H_2adc-based MOF with permanent and experimentally assessed porosity was found with Zr-HHUD-1, which is structurally analogous to UiO-66,[5,15] followed by NUS-36, another Zr-based MOF,[16] and the Hf- and Ce-based MOFs Hf-HHUD-1 and Ce-HHUD-1.[6,7,17] The M-HHUD-1 MOFs showed very interesting gas sorption properties for CO_2 and H_2 with high values for the isosteric heat of adsorption, an increase in hydrophilicity compared to fumarate based MOFs and exhibited potential for the chemisorption of hazardous halogen vapors, like bromine and iodine.[5–7]

While the isoreticular synthesis approach has been successfully used for the synthesis of IRMOF and UiO-66 analogous adc-based MOFs, no synthesis based on the MIL-53 structure, which also lends itself for the isoreticular MOF synthesis approach, has been reported yet.[5,12,16] The MIL-53 secondary building unit (SBU) consists of M^{3+}-chains (M = Al, In, Ga, Cr, Fe) with *trans* bridging μ-OH groups (Fig. 1a) which are interconnected through bifunctional linkers to a 3-dimensional network.[19–22] MIL-160, CAU-10-H and CAU-23 are MOFs closely related to MIL-53 with SBUs consisting of *cis* connected or a mixture of *cis* and *trans* connected μ-OH groups, respectively (Fig. 1b and c).[23–25]

cis-Only and mixed *cis/trans* connected μ-OH groups have so far usually been achieved through the use of V-shaped linker molecules, like furandicarboxylate, isophthalate and thiophenedicarboxylate, respectively. Linear ligands like terephthalate or fumarate yielded only *trans*-connected μ-OH groups with MIL-53 type structures (Scheme 1).[19,20,24,25]

The MOFs Al-MIL-53, MIL-160, CAU-10-H and CAU-23 are frequently investigated for their properties such as structural flexibility,[26] sensing and selective separation of volatile organic compounds like xylene,[27–29] high thermal and water stability with high water uptake and promising gas sorption properties with high uptakes for H_2, CO_2 and SO_2 and potential for the separation of gases.[25,30,31]

Herein we present the successful synthesis and characterization of a new In-adc MOF, named HHUD-4 which shows *cis*-μ-OH connected {InO_6} octahedra, unexpected for linear ligands.

Experimental

Materials and methods

All chemicals were obtained from commercial sources and used without further purification. The starting material $In(NO_3)_3·xH_2O$ has no stoichiometrically defined water content and is sold as an '*x* hydrate'. At the same time this compound is hygroscopic. Attempts to quantify the water amount with Karl-Fischer titration yielded 3.5–5 water molecules per formula unit. Coulometric Karl-Fischer titration was performed with an ECH/Analytik Jena AQUA 40.00 Karl Fischer titrator
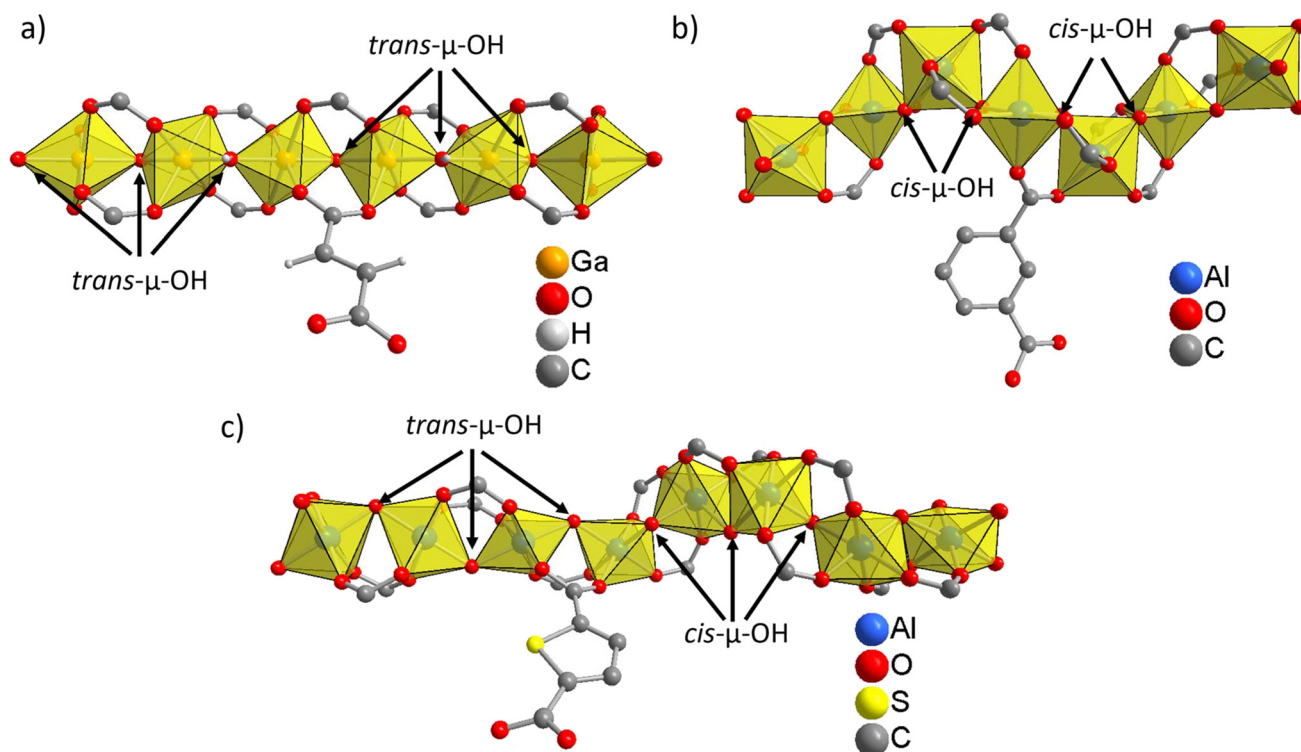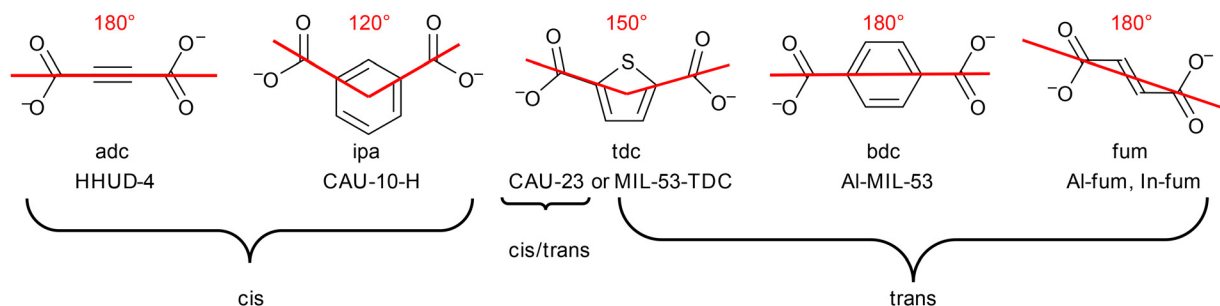

Fig. 1 Illustration of {MO_6} chains with different μ-OH connectivity: (a) Ga-fum (Ga-MIL-53(fum)) (straight chains; *trans*-μ-OH), (b) CAU-10-H (helical chains; *cis*-μ-OH) and (c) CAU-23 (straight and helical chains; *trans*−*cis*-μ-OH). The structures were redrawn from the cif files 1838533 (Ga-fum), 1454066 (CAU-10-H) and 1878820 (CAU-23) deposited at the CCDC.[18,20,25]

Scheme 1 Illustration of linker molecules relevant in this work, their opening angles and the resulting MOFs with their *cis*- and/or *trans*-μ-OH connectivity of the {MO_6} octahedra.[19,20,24,25] (ipa = isophthalate, tdc = thiophenedicarboxylate, bdc = benzenedicarboxylate, fum = fumarate).

equipped with a headspace module. Thermogravimetric analysis was carried out on a Netzsch TG 209 F3 Tarsus in the temperature range from 30 °C to 600 °C with a heating rate of 5 K min^{-1} under a nitrogen atmosphere. Powder X-ray diffraction (PXRD) patterns were recorded on a Bruker D2 Phaser powder diffractometer with a flat silicon, low background sample holder, at 30 kV, 10 mA with Cu-Kα radiation (λ = 1.5418 Å). The most intense reflection in each diffractogram was normalized to 1. The simulated PXRD pattern was calculated with the MERCURY software.[32] Supercritical drying was carried out on a Leica EMPCD 300 over 18 exchange cycles with CO_2. Raman spectra were acquired using a Bruker MultiRAM-FT Raman spectrometer equipped with a Nd:YAG-laser (λ_{exc} = 1064 nm). The spectra were obtained for 2500 scans with a laser intensity of 50 mW. Scanning electron microscopy (SEM) images were acquired on a JEOL JSM-6510 Advanced electron microscope with a LaB$_6$ cathode at 5–20 keV. The microscope was equipped with an Xflash 410 silicon drift detector for energy-dispersive X-ray spectroscopy. Adsorption data for N_2 at 77 K (liquid nitrogen bath) were collected on a Quantachrome NOVA 4000 gas adsorption analyzer. Volumetric gas sorption experiments for H_2, CO_2 and CH_4 were carried out on a Quantachrome Autosorb iQ MP at 77, 87 and 100 K for H_2 and 273 and 293 K for CO_2 and CH_4, respectively. Vapor sorption isotherms for H_2O, benzene, cyclohexane and hexane were measured on a Quantachrome VSTAR vapor sorption analyzer at 293 K. For activation the supercritically dried HHUD-4 was outgassed at room temperature for a minimum of 6 h while the In-fum sample was outgassed at 100 °C for at least 6 h before the sorption experiments.

Single crystal X-ray diffraction

Suitable crystals were carefully selected under a polarized-light microscope, covered with protective oil and mounted on a cryo-loop. The data were collected on a Bruker Kappa APEX 2 CCD X-ray diffractometer with a microfocus sealed tube, Mo-Kα radiation (λ = 0.71073 Å), and a multi-layer mirror monochromator; data collection was done at 140 ± 2 K using ω-scans, cell refinement was performed with APEX2,[33] data reduction was performed with SAINT[34] and experimental adsorption correction was done with SADABS.[35] Structure analysis and refinement: the structures were solved by direct methods (SHELXT-2015)[36,37] and full-matrix least-squares

refinements on F^2 were carried out using the SHELXL-2017/1 program package. The hydrogen atoms for μ-OH were positioned geometrically (with O–H = 0.95 Å) and refined using a riding model (AFIX 43 with $U_{iso(H)}$ = 1.2U_{eq}).

Highly disordered solvent molecules have been masked with the SQUEEZE option in PLATON.[38,39] For crystal 1 the resulting solvent accessible volume of 738 Å^3 per unit cell contained 243 electrons, which may correspond to about 9 ethanol (26 electrons each) or up to 24 water molecules (10 electrons each) as the solvent of crystallization per unit cell or about 2.3 ethanol or 6 water molecules per asymmetric unit (Z = 4). For crystal 2 the resulting solvent accessible volume of 735 Å^3 per unit cell contained 158 electrons, which may correspond to about 6 ethanol or 16 water molecules per unit cell or about 1.5 ethanol or 4 water molecules per asymmetric unit.

Crystal data and details on the structure refinement are given in Table 1. Details about selected bond distances and angles are given in Section S8, ESI.† Graphics were drawn with the program DIAMOND.[40]

The crystallographic data for the structure have been deposited with the Cambridge Crystallographic Data Centre (CCDC numbers 2220400 and 2220401†).

Synthesis of HHUD-4 (In-adc)

186 mg (0.5 mmol for x = 4) of In(NO$_3$)$_3$·xH$_2$O and 57 mg (0.5 mmol) of acetylenedicarboxylic acid were sequentially dissolved in 700 μL de-ionized water in a 20 mL glass vial. Afterwards 10 mL of ethanol were added leading to a white dispersion, which was placed in a programmable oven at 70 °C for 48 h with a heating and cooling step of 3 h each to obtain colorless crystals in the form of an elongated square bipyramid (also named elongated octahedron, pencil cube or 12-faced pencil cube)[41] (see Fig. S3 and S4, ESI†). For the purification of the bulk material the mother liquor was then exchanged against fresh ethanol (10 mL) twice a day for three days to remove unreacted educts. Afterwards the solvent was removed *via* supercritical drying with CO_2 yielding 92 mg (75%) of a white precipitate.

Synthesis of In-fum

The synthesis of In-fum was carried out following a modified literature reported procedure by Zhang *et al.*[20] 186 mg

Table 1 Crystal data and structure refinement details of HHUD-4

	Crystal 1	Crystal 2
CCDC no.	2220400	2220401
Chemical formula	C_4HO_5In	C_4HO_5In
M_r (g mol^{-1})	243.87	243.87
Crystal system, space group	Tetragonal, $P4_122$	Tetragonal, $P4_322$
Temperature (K)	140	140
$a = b$ (Å)	9.8021 (7)	9.8015 (9)
c (Å)	12.812 (1)	12.7970 (14)
V (Å^3)	1231.0 (2)	1229.4 (3)
Z	4	4
μ (mm^{-1})	1.90	1.90
$d_{calc.}$ (g cm^{-3})	1.316	1.318
F (000)	456	456
Crystal size (mm)	$0.31 \times 0.18 \times 0.17$	$0.24 \times 0.22 \times 0.20$
T_{min}, T_{max}	0.882, 1.000	0.578, 0.685
Measured, independent, observed reflections	8314, 1284, 1266	7274, 1889, 1843
Parameters, restraints	47, 0	47, 0
R_{int}	0.023	0.018
$(\sin \theta/\lambda)_{max}$ (Å^{-1})	0.628	0.716
R, w$R(F^2)$, S $[F^2 > 2\sigma(F^2)]^a$	0.0094, 0.0245, 1.127	0.0127, 0.0335, 1.084
R, w$R(F^2)$, S [all data]^a	0.0095, 0.0246, 1.127	0.0131, 0.0336, 1.084
$\Delta\rho_{max}, \Delta\rho_{min}^b$ (e Å^{-3})	0.21, −0.30	0.90, −0.24
Absolute structure parameter^c	−0.017 (17)	−0.009 (15)

$^a R_1 = [\sum(||F_o| - |F_c||)/\sum|F_o|]$; w$R_2 = [\sum[w(F_o^2 - F_c^2)^2]/\sum[w(F_o^2)^2]]^{1/2}$. Goodness-of-fit $S = [\sum[w(F_o^2 - F_c^2)^2]/(n - p)]^{1/2}$. ^{b} Largest difference peak and hole. ^{c} Flack parameter.[42–45]

(0.5 mmol for $x = 4$) of $In(NO_3)_3 \cdot xH_2O$, 58 mg (0.5 mmol) of fumaric acid and 10 mL ethanol were mixed in a 20 mL glass vial. The vial was placed in a programmable oven at 70 °C with a heating and cooling step of 3 h each to obtain a white precipitate. The precipitate was washed with fresh ethanol (10 mL) twice a day for three days and afterwards dried under vacuum at 60 °C to obtain 85 mg (69%) of a white powder.

Results and discussion

Synthesis and the crystal structure of HHUD-4

HHUD-4 (In-adc) was obtained through the reaction of $In(NO_3)_3 \cdot xH_2O$ with acetylenedicarboxylic acid (H_2adc) in a mixture of ethanol and de-ionized water at 70 °C. This synthesis yielded colorless elongated square-bipyramidal crystals of the formula $[In(OH)(adc)] \cdot$solvent. The experimental morphology of the crystals (Fig. S3 and S4, ESI†) matched the calculated morphology from the crystal structure data using the Bravais, Friedel, Donnay and Harker (BFDH) algorithm embedded in MERCURY (Fig. S3b†).[32]

The phase purity and the retention of the structure through the washing and activation procedures of the bulk HHUD-4 material were confirmed through a positive match between the simulated powder X-ray diffraction (PXRD) pattern and the experimental pattern of the as-synthesized material (Fig. 2). For activation, the solvent has been exchanged with fresh ethanol three times before the sample was dried with supercritical CO$_2$. Afterwards the sample was outgassed at room temperature under dynamic vacuum for at least 6 h. No phase change or loss of crystallinity of the bulk material could
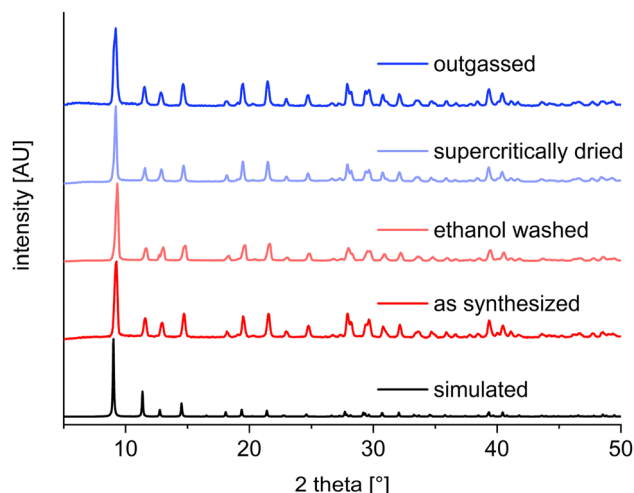

Fig. 2 Comparison of the simulated and experimental PXRDs of HHUD-4 after sequential activation steps.

be observed after any of the sequential activation steps by PXRD (Fig. 2).

HHUD-4 crystallizes in enantiopure crystals in the chiral, enantiomorphic tetragonal space groups $P4_122$ or $P4_322$, most likely as a racemic conglomerate.[46,47] The asymmetric unit consists of one In(III) ion, one μ-OH-group and a half of an adc^{2-} linker molecule in addition to strongly disordered solvent molecules belonging to ethanol and/or water, which have been removed with the SQUEEZE command in PLATON.[38,39] Each In(III) ion has a slightly distorted octahedral coordination with In–OH bond lengths of 2.074(1) Å and In–O

bond lengths between 2.165(1) and 2.174(1) Å to the carboxylate O-atoms (Fig. 3). The acetylene (C2–C2^{iv}) bond distance with a length of 1.183(4) Å corresponds to the expected triple bond character.[48] The preservation of the C–C triple bond has been further confirmed by Raman spectroscopy (Fig. S1†) through a strong band at 2238 cm^{-1}.

Each In(III) ion is connected to two neighboring In(III) ions along the infinite {InO$_6$} secondary building units through two *cis*-bridging μ-OH groups and four bridging carboxylate adc^{2-} units which also link the adjacent infinite {InO$_6$} strands, leading to a 3-dimensional network with square channels (Fig. 4a). The *cis*-μ-OH connection of the In atoms leads to fourfold helical chains with either a right-handed 4$_1$ or a left-handed 4$_3$ helix around the crystallographic 4$_1$ or 4$_3$ axis, respectively. The 4$_1$ or 4$_3$ axis runs parallel to the *c*-axis and passes through the oxygen atoms of the μ-OH groups (Fig. 4b). From six investigated single crystals three crystallized in the space group *P*4$_1$22 and the other three in *P*4$_3$22 (Table 1). The Flack parameters are close to zero, which supports the correct absolute structure assignment and in combination with normal atom temperature factors and no molecular disorder, excludes the fact that chains of opposite helicity are present within the investigated crystals in a significant amount.[42–45]

Fourfold helices were also seen in the structurally closely related MOFs [Al(OH)(isophthalate)] (CAU-10-H) and [Al(OH)(furandicarboxylate)] (MIL-160).[23,24] Both MOFs have V-shaped ligands with opening angles of ~120° (Scheme 1), correlated to the *cis*-μ-OH connectivity. In dry CAU-10-H the structure is centrosymmetric in the space group *I*4$_1$/*amd* with both 4$_1$ and 4$_3$ helices in the crystal. Upon water uptake, CAU-10-H experiences a reversible phase change to a non-centrosymmetric structure in the space group *I*4$_1$, proven by second harmonic generation.[18] In contrast HHUD-4 is the first literature-reported MOF to utilize a linear ligand to obtain helical chains
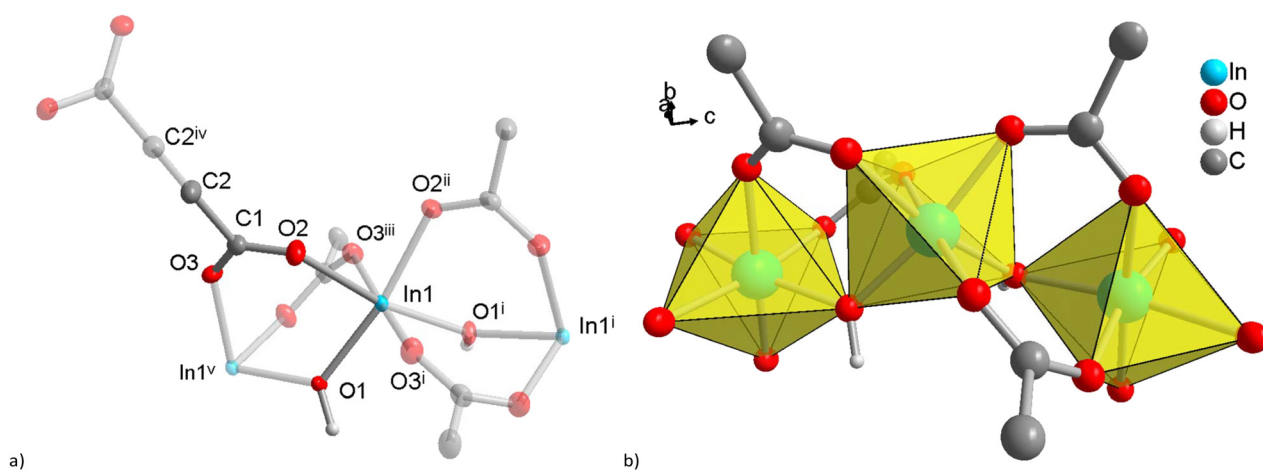

Fig. 3 (a) Extended asymmetric unit of HHUD-4 (50% thermal ellipsoids, H atoms with arbitrary radii). Symmetry transformations: (i) −*y* + 1, *x*, *z* + 1/4; (ii) −*x* + 1, *y*, −*z* + 1; (iii) *y*, *x*, −*z* + 3/4; (iv) *x*, −*y* + 2, −*z* + 1/2; (v) *y*, −*x* + 1, *z* − 1/4. (b) Section of the infinite {InO$_6$} SBU with the octahedral coordination of the In(III) ions emphasized by polyhedra.
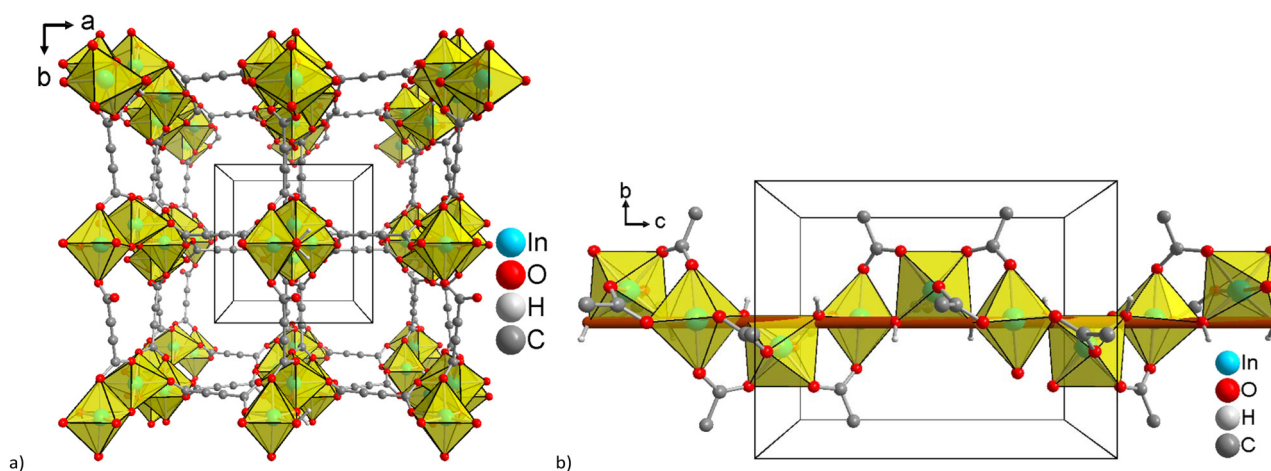

Fig. 4 (a) 3D-network structure and (b) the right-handed 4$_1$ helix alongside the crystallographic 4$_1$ axis (brown) which is colinear to the *c*-axis in HHUD-4. The coordination environment of the In(III) ion is highlighted as yellow octahedra.

through *cis*-bridging-μ-OH groups. Thereby, HHUD-4 contradicts the general assumptions accepted, so far, for *cis*- and *trans*-μ-OH connectivity in infinite {MO$_6$} SBUs. From the MOFs known in the literature it was assumed that linear ligands would lead to *trans*-bridging-μ-OH groups and MIL-53-type structures.[30,49–51] On the other hand V-shaped ligands with an opening angle of ~120° between both carboxylate groups would result in *cis*-μ-OH bridging as seen in MIL-160 and CAU-10-H,[23,24] whereas V-shaped ligands with an opening angle of ~150° can either give a mixture of *trans* and *cis* as in CAU-23 or *trans*-μ-OH bridging only as in MIL-53-TDC (for longer ligands).[25,52]

Due to the linearity of the adc linker, the structure of HHUD-4 differs slightly from the CAU-10-H structure in the orientation of the helical chains to each other. While there are both 4$_1$ and 4$_3$ chains with an image/mirror image relationship with each other in both CAU-10-H(dry) and CAU-10-H(H$_2$O), in HHUD-4 the helical {MO$_6$}-chains have the same sense of rotation and run exactly parallel to each other (Fig. 5).

The MOF HHUD-4 consists of **square layers** in the direction of the *c*-axis (Fig. 4a and Fig. 6a). The topological analysis of the structure with ToposPro[53,54] and the Topcryst database[55,56] yielded the **sql**-topology in the cluster representation, which is a commonly found topology for MOFs with over 9000 structures in the Topcryst database.

The solvent depleted 3D network has potential porosity from the square channels running along the *c* axis with diagonals of about 9.2 Å and widths of about 6.6 × 6.6 Å² (between the van der Waals surfaces). Smaller channels run along the

crystallographic *a* and *b* axes with cross sections of about 5.0 × 4.2 Å² (Fig. 6b).

Gas sorption studies in HHUD-4 and In-fum

For the gas sorption studies, HHUD-4 has been activated by solvent exchange with fresh ethanol three times before drying with supercritical CO$_2$ and outgassing at room temperature under dynamic vacuum (<30 mbar) for at least 6 h.

Interestingly, without any changes to the synthesis and activation procedures, volumetric nitrogen sorption experiments for multiple samples of HHUD-4 at 77 K yielded BET surface areas in the range from about 660 up to 940 m² g⁻¹ (Table S1†), with surface areas of about 700 m² g⁻¹ showing the highest reproducibility. The nitrogen sorption isotherms (Fig. 7) are of type I with a very minor H4 hysteresis which may stem from inter-particle voids of the aggregated crystals. As a point of reference for HHUD-4 the related MOF indium fumarate, In-fum, was synthesized. In-fum has a linear, albeit kinked linker with four carbon atoms and also a C–C multiple (double) bond (Scheme 1). As a further difference, the {InO$_6$} octahedra are connected by *trans*-μ-OH bridges. Still their similarity should allow the assessment of the role of the triple *vs.* double bond. Based on the isostructural Ga-fum framework the In-fum framework (for which no crystal structure was deposited)[20] also has square channels running along the *a* axis. From the Ga-fum structure and with a covalent radius of In 0.2 Å larger than for Ga, the channel diagonals in In-fum were estimated to be about 8.0 Å and widths to be about 6.2 × 6.2 Å² (between the van der Waals surfaces). Smaller channels in In-

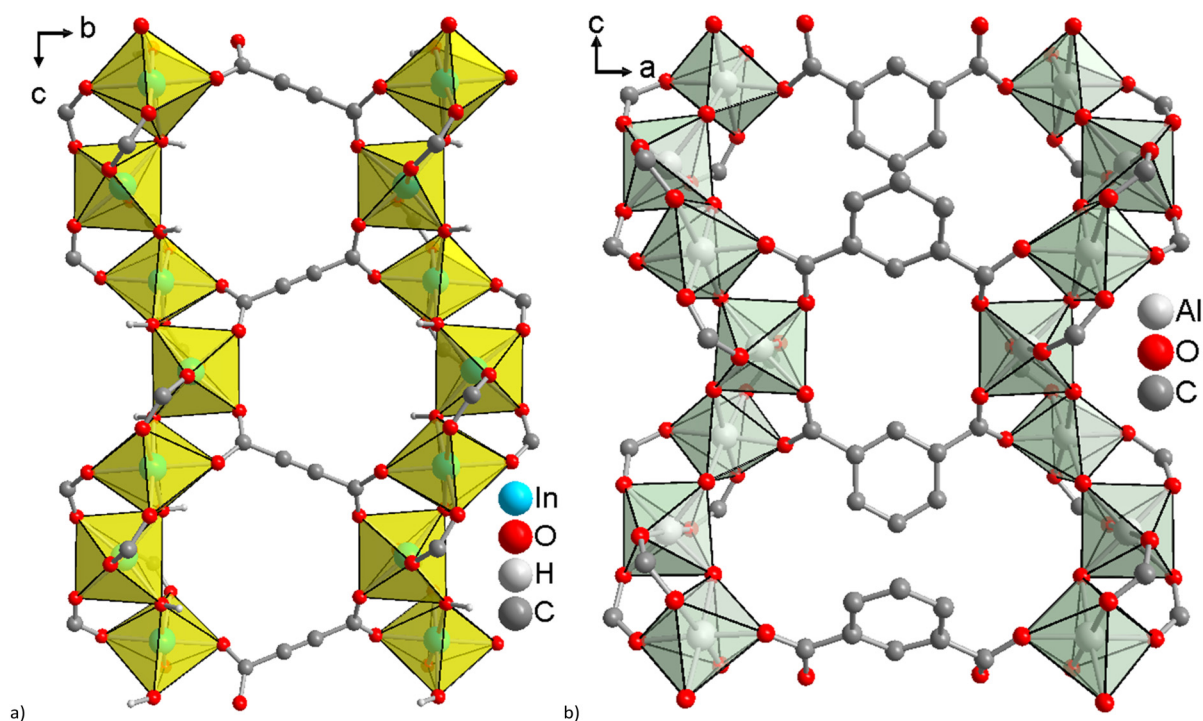**Fig. 5** (a) The parallel {InO$_6$}-helices in HHUD-4 and (b) the mirrored {AlO$_6$}-helices in CAU-10-H(H$_2$O) (H$_2$O molecules not shown for clarity) similar to those in CAU-10-H(dry). The structure of CAU-10-H(H$_2$O) is redrawn from the cif file 1454066 deposited at the CCDC.[24]
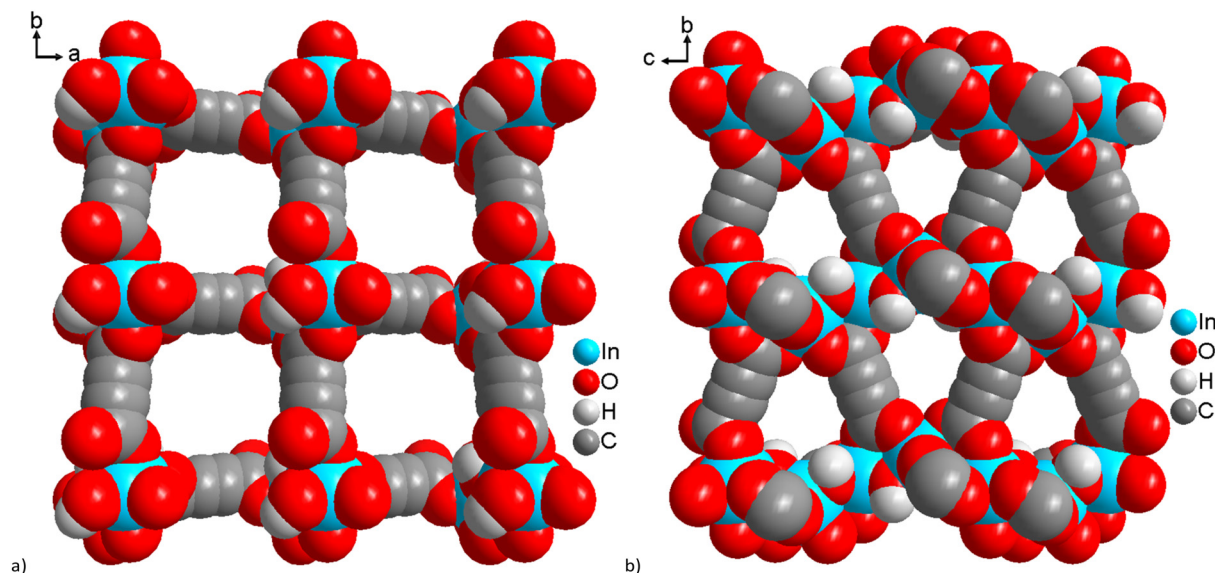
Fig. 6 Channels along the *c*-axis (a) and along the *a*- or *b*-axis (b) in HHUD-4.
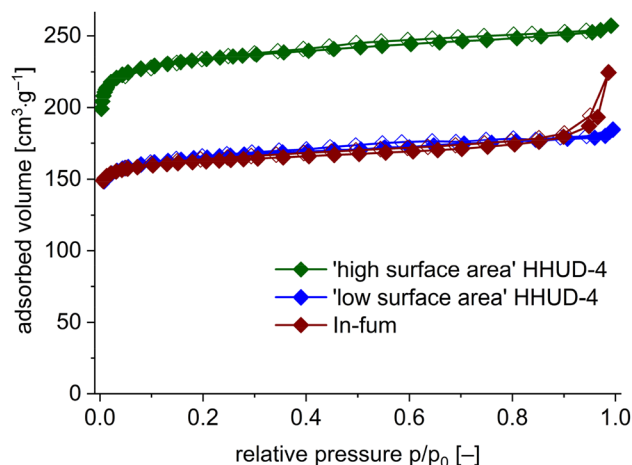

Fig. 7 Volumetric N_2 sorption experiments of high and low surface area HHUD-4 and In-fum at 77 K (filled symbols for adsorption, empty symbols for desorption).

fum run perpendicular to the *a* axis with estimated cross sections of about 4.2 × 1.5 Å^2 (Fig. S7;† compared to Fig. 6 for HHUD-4). Due to the superior thermal stability of the fumarate linker, the bulk In-fum material was not supercritically dried and instead outgassed at 100 °C under high vacuum (<30 mbar) (PXRD, Fig. S2†).

With a BET surface area of about 660 m^2 g^{-1}, In-fum shows a similar surface area to the 'low surface area' samples of HHUD-4, while the 'high surface area' sample of HHUD-4 is comparable to MIL-53-fum (1020 m^2 g^{-1}).[30]

Due to the better reproducibility, the 'low surface area' HHUD-4 with about 660 m^2 g^{-1} was further studied alongside In-fum for their comparative gas sorption capabilities of CO_2, CH_4 and H_2 at varying temperatures (Fig. 8 and Table S2,

ESI†). With a total CO_2 uptake of 2.74 mmol g^{-1} at 293 K and 1 bar, HHUD-4 not only adsorbs about 56% more CO_2 than In-fum (1.76 mmol g^{-1}) but also surpasses the other known adc-based MOFs M-HHUD-1 (M = Zr, Ce and Hf)[5–7] and NUS-36,[16] making HHUD-4 the adc-based MOF with the highest capacity for CO_2. HHUD-4 and M-HHUD-1 have similar surface areas. The CO_2 uptake of HHUD-4 is also comparable to that of the structurally related Al-MOFs MIL-53 (2.11 mmol g^{-1}), CAU-10-H (2.76 mmol g^{-1}) and Al-fum (2.52 mmol g^{-1}) but lower than that of MIL-160 (4.22 mmol g^{-1}) and CAU-23 (3.97 mmol g^{-1}).[31,57] The high CO_2 uptake of HHUD-4 in comparison with In-fum illustrates the advantageous role of the C–C triple bond for CO_2 adsorption. The isosteric heat of adsorption for HHUD-4 and In-fum was calculated from the isotherms obtained at 273 and 293 K (Fig. 9). The zero-coverage heat of adsorption Q_{st}^0 of about 29 kJ mol^{-1} for HHUD-4 is lower than that of other literature reported adc-MOFs (39–60 kJ mol^{-1})[5–7] but comparable to that of MIL-160, CAU-10-H and MIL-53(Al) (25–33 kJ mol^{-1}).[58–60]

The CH_4 adsorption capacity of HHUD-4 at 293 K is 0.72 mmol g^{-1}, which is an increase of about 29% compared to that of In-fum (0.56 mmol g^{-1}), thus bringing HHUD-4 into the range of the above-mentioned Al-MOFs (0.57–1.14 mmol g^{-1}).[31,61,62] In contrast to the maximum uptake both HHUD-4 and In-fum show a significantly higher Q_{st}^0 for CH_4 of about 26 and 30 kJ mol^{-1} than MIL-53, Al-fum, MIL-160, CAU-23 and CAU-10-H (8–16 kJ mol^{-1}),[31,62] indicating attractive interactions between the In-based MOFs and CH_4. The kinetic diameter of CH_4 is 3.8 Å. A plausible explanation is that the suitably-shaped C≡C-triple and C=C-double-bond-lined windows of the small channels along the *a* and *b* axes in HHUD-4 of ~5.0 × 4.2 Å^2 and in In-fum of ~4.2 × 1.5 Å^2, respectively, (Fig. 6b and Fig. S7b†) offer several $(CH_4)CH\cdots\pi$ contacts with a significant cumulative strength.
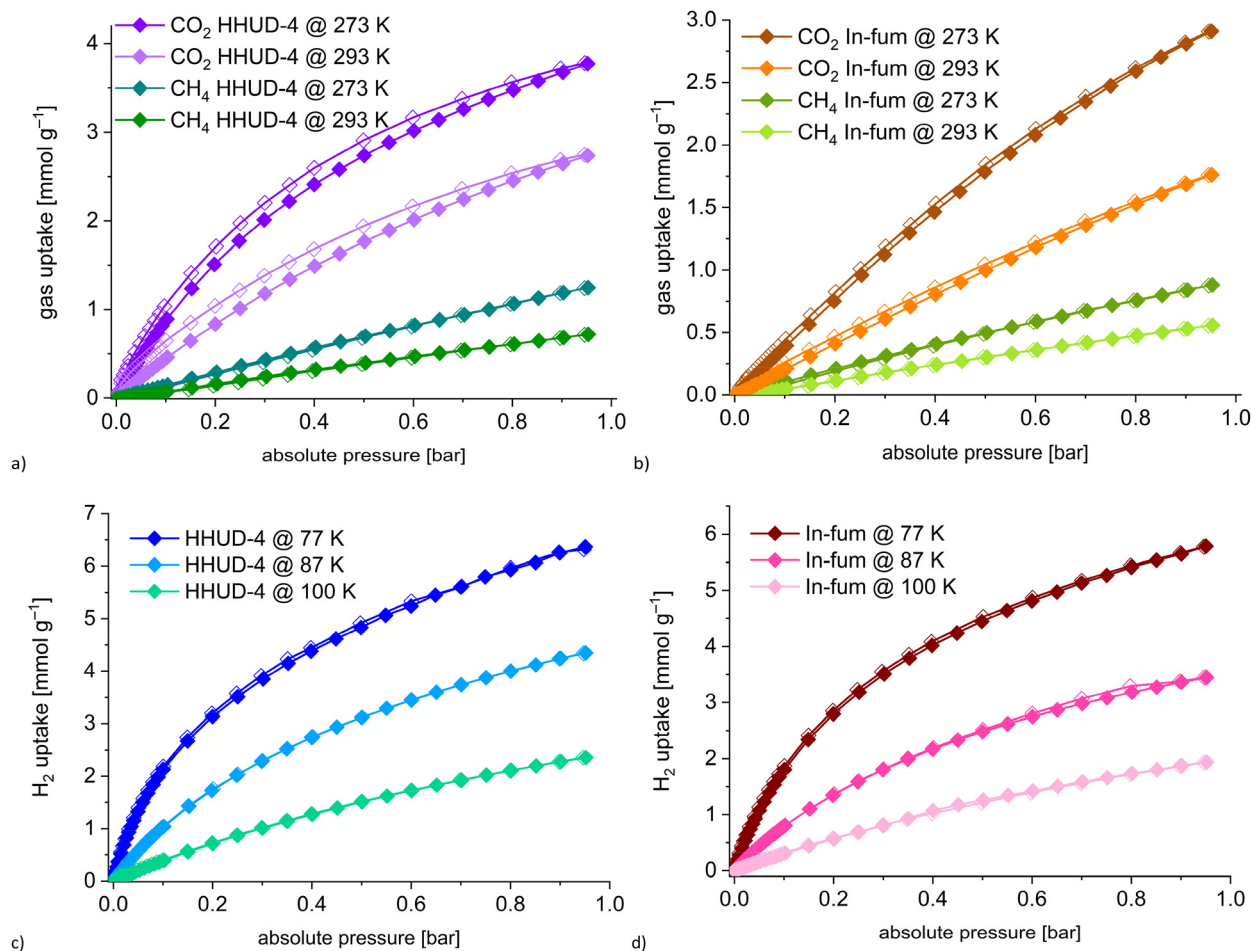
Fig. 8 CH_4 and CO_2 sorption isotherms at 273 and 293 K and H_2 sorption isotherms at 77, 87 and 100 K for HHUD-4 (a and c) and In-fum (b and d), respectively (filled symbols for adsorption, empty symbols for desorption).
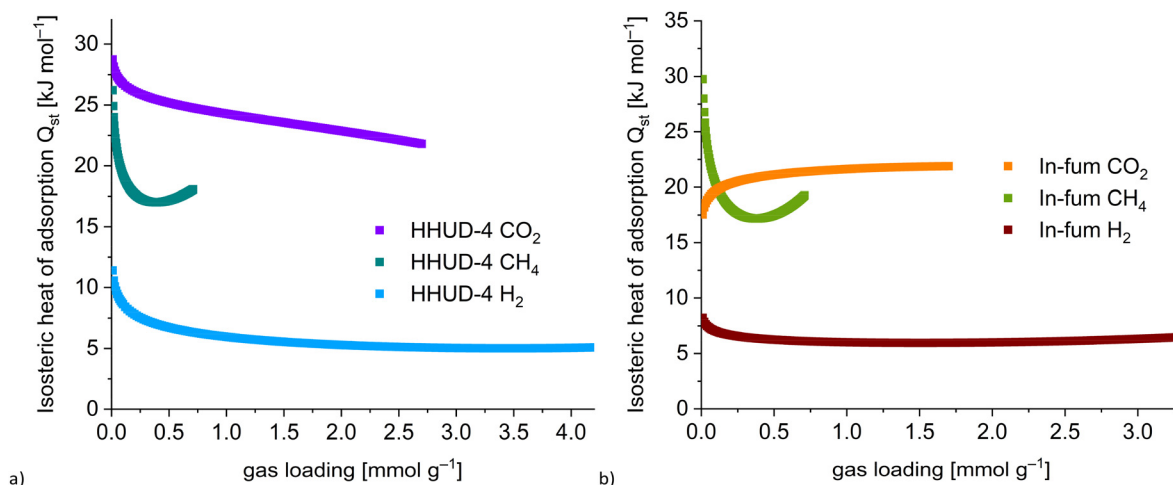

Fig. 9 Isosteric heat of adsorption of HHUD-4 (a) and In-fum (b) for CO_2, CH_4 (from adsorption data at 273 and 293 K) and H_2 (from adsorption data at 77 and 87 K).

The selectivities for CO_2 *versus* CH_4 were calculated with variable molar fractions at 273 K or 293 K and 1 bar with the 3PSim software (see Section S4† for further details).[63] IAST (ideal adsorbed solution theory) calculations with Toth-fitted isotherms yielded selectivities of 6.0 (273 K) or 6.9 (293 K) for HHUD-4 and 4.4 (273 K) or 3.5 (293 K) for In-fum at a molar

fraction of 0.5, respectively. An IAST selectivity of 6.9 with HHUD-4 for CO_2/CH_4 separation is also better than that of Al-fum (4.5, 273 K),[64] CAU-23 (5.3, 293 K),[31] MIL-160 (6, 295 K)[65] and MIL-53 (6.3, 298 K).[66]

The H_2 adsorption capacity at 77 K and 1 bar is 10% higher for HHUD-4 with 6.36 mmol g^{-1} than for In-fum (5.78 mmol g^{-1}). For both In-MOFs the H_2 adsorption isotherms show no saturation at 1 bar (Fig. 8). More interestingly HHUD-4 exhibits a high near zero coverage Q_{st}^0 of 11.4 kJ mol^{-1}, which is an increase of about 40% compared to In-fum (8.2 kJ mol^{-1}). This value puts HHUD-4 near the MOFs with the highest literature

reported isosteric heat of adsorption for H_2 such as SNU-15′ (15.1 kJ mol^{-1}),[67] Ni(dhtp) (12.9 kJ mol^{-1}, dhtp = 2,5-dihydroxy-terephthalate)[68] and $Zn_3(bdc)_3[Cu(pyen)]\cdot(DMF)_5(H_2O)_5$ (12.3 kJ mol^{-1}, bdc = 1,4-benzenedicarboxylate and pyenH$_2$ = 5-methyl-4-oxo-1,4-dihydro-pyridine-3-carbaldehyde).[69] Thus, HHUD-4 presents the advantageous properties of C≡C triple bonds for hydrogen storage, similar to the results previously reported by Farha *et al.* for triple-bond containing large ligands.[70]

Vapor sorption studies in HHUD-4 and In-fum

Toxic gases and vapors of volatile organic compounds (VOCs) in the atmosphere are a major concern and their removal, degradation and the separation of mixtures with MOFs is of scientific interest.[71–73] Benzene, cyclohexane and *n*-hexane are among the VOCs that can be found indoors and as they pose health risks their removal is of importance. Benzene is commonly regarded as the most toxic indoor VOC, as it cannot be biodegraded and thus is potentially cancerogenic,[74,75] but also *n*-hexane, which metabolizes to the nerve-damaging and toxic 2,5-hexanedione,[76,77] is of significance for removal. Additionally, the separation and purification of benzene and cyclohexane with MOFs is of particular interest, since the current industrial processes such as distillation and extraction are energy intensive.[78–80] Besides open metal sites, properties such as double or triple bonds proved to be advantageous for the adsorption of benzene due to their capability to interact *via* π···π interactions with benzene.[78] Thus, HHUD-4 and In-fum are interesting candidates for such a comparative separation process to elucidate the role of the triple bond in the framework surface.

In vapor sorption experiments for benzene, cyclohexane and *n*-hexane at 293 K, HHUD-4 and In-fum show an overlap of type I(a) or I(b) isotherms at lower pressures and type II isotherms at higher pressures (Fig. 11). Additionally, a very wide hysteresis can be observed for the uptake of benzene in both
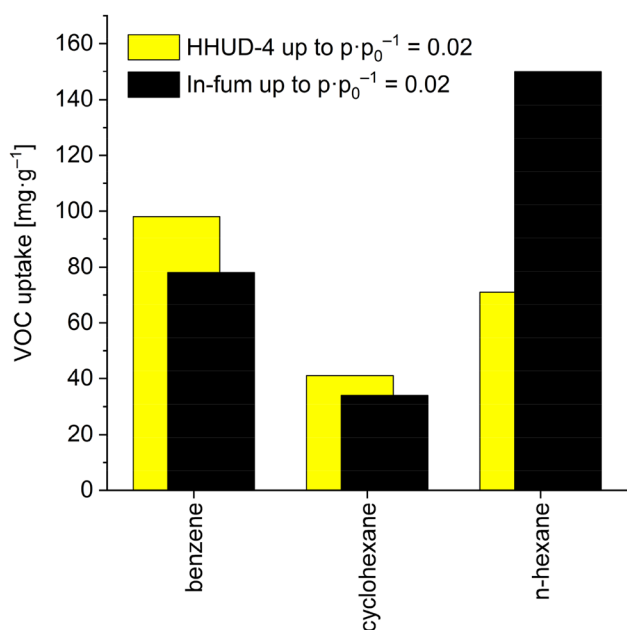

Fig. 10 Benzene, cyclohexane and *n*-hexane uptake capacity of HHUD-4 and In-fum at a relative pressure of up to $p/p_0 = 0.02$ at 293 K (specific values in Table S9†).
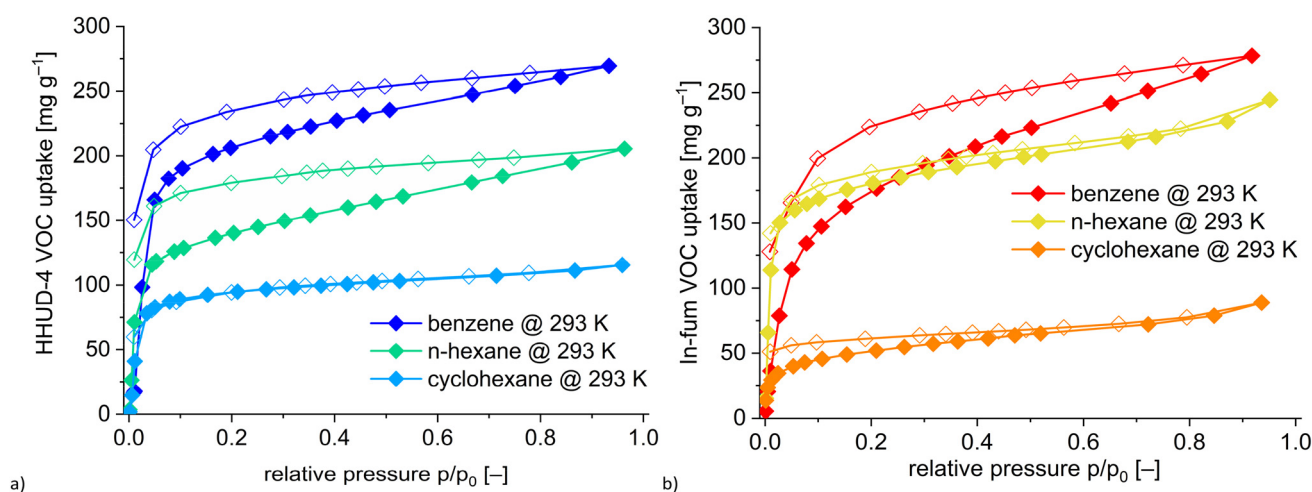

Fig. 11 Benzene, cyclohexane and *n*-hexane vapor sorption isotherms at 293 K for (a) HHUD-4 and (b) In-fum (filled symbols for adsorption, empty symbols for desorption).

MOFs and cyclohexane in HHUD-4. Wide hystereses in benzene adsorption experiments with MOFs are interpreted as host–guest $\pi\cdots\pi$ or C–H$\cdots\pi$ interactions in the literature.[81] The desorption of cyclohexane and n-hexane in In-fum features a small hysteresis, while no hysteresis can be seen for cyclohexane in HHUD-4, indicating few host–guest interactions and few restrictions regarding the movements of the molecules out of the pores. The three molecules have a kinetic diameter of 5.85 Å for benzene, 6 Å for cyclohexane, and 4.3 Å for linear n-hexane.[82] The critical molecular dimension for diffusion through cylindrical pore cross sections is the width of 6.628 Å for benzene, 6.580 Å for cyclohexane and 4.536 Å for n-hexane[83] which are all smaller than the pore diagonals in both In-MOFs (*vide supra*). Remarkably, cyclohexane has significantly smaller uptakes in both MOFs, in particular in In-fum. The high uptake of benzene can be rationalized through its $\pi\cdots\pi$ or C–H$\cdots\pi$ interactions with the C≡C-triple and C=C-double bonds of the frameworks. Also, benzene has a higher density (0.876 g cm^{-3}) in a liquid-like adsorbate state for a given pore volume than cyclohexane (0.779 g cm^{-3}) or n-hexane (0.655 g cm^{-3}) at 293 K. There is no special adsorbate–adsorbent interaction for n-hexane. Hence its relatively high uptake (even higher than benzene in In-fum at low pressure) can only be traced to having the smallest critical dimension among the three VOCs (*vide supra*). Thereby, n-hexane can enter narrow pores and pore window regions which are not accessible for the larger cyclohexane and benzene molecules.

HHUD-4 and In-fum show steep VOC vapor uptake steps in the low pressure region with HHUD-4 reaching relative uptakes of its maximum capacity of about 71, 77 and 63% for benzene, cyclohexane and n-hexane at a relative pressure p/p_0 of 0.1, respectively (Fig. 10 and Table S9,† p_0 = 95 mbar for benzene, 101 mbar for cyclohexane and 160 mbar for n-hexane). Even at the very low relative pressure p/p_0 of 0.02, HHUD-4 still shows a moderately high adsorption capacity of about 35 to 36% for each VOC vapor, which is better than In-fum (Fig. 10 and Table S9†). On the other hand, for the particularly toxic n-hexane, In-fum shows a remarkable uptake of 150 mg g^{-1} (61%) at the low relative pressure p/p_0 of 0.02. Since high adsorption capacities at low relative pressures are important for the removal of VOC traces, both HHUD-4 and In-fum are interesting materials for the indoor capture and removal of VOCs.

Selectivities for benzene/cyclohexane, benzene/n-hexane and n-hexane/cyclohexane were calculated for a 50 : 50 (v/v) mixture at 293 K and variable vapor pressure with the 3PSim software (see Section S6† for further details). IAST (ideal adsorbed solution theory) calculations yielded selectivities below 5 in the low-pressure area for both MOFs (Fig. 12). While no increase in selectivity can be observed for either MOF for benzene/n-hexane mixtures, for benzene/cyclohexane mixtures the selectivity increases with pressure to 17 for HHUD-4 and 22 for In-fum at 90 mbar (Fig. 12). The preference for benzene is probably due to $\pi\cdots\pi$ interactions between the aromatic benzene ring and the double or triple bonds of
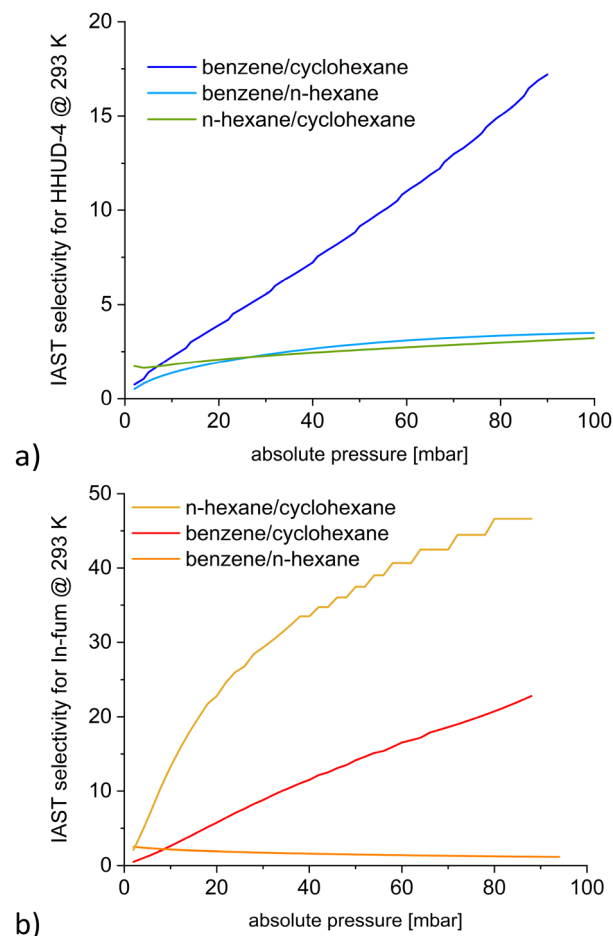
a)

b)

Fig. 12 IAST selectivities for benzene/cyclohexane, benzene/n-hexane and n-hexane/cyclohexane mixtures for (a) HHUD-4 and (b) In-fum.

the fumarate or acetylenedicarboxylate linker.[81] Remarkably, for n-hexane/cyclohexane mixtures in In-fum a rapidly increasing IAST selectivity with pressure to about 47 at 90 mbar was calculated (Fig. 12b). In the absence of special adsorbate–adsorbent interactions for both C$_6$-alkane molecules, when the smaller n-hexane enters the narrow pores and their vicinities, the larger cyclohexane is even more effectively excluded.

The stability of HHUD-4 and In-fum against benzene, cyclohexane and n-hexane was confirmed with PXRD and N$_2$ sorption experiments, showing no changes in the PXRD patterns and only slight increases or decreases in the adsorbed volume and the surface area for both MOFs (Fig. S18–S21 and Table S10, ESI†). With good stabilities and selectivities of above 15, both HHUD-4 and In-fum are promising candidates for the separation of benzene/cyclohexane mixtures and In-fum for the separation of n-hexane/cyclohexane mixtures in the industry, where selectivities higher than 3 would already be sufficient for application in such processes.[76,84]

In addition to vapor sorption experiments for VOCs, water sorption studies were also carried out. The sorption capabilities of water are interesting for the possible application of MOFs as adsorbents in water driver adsorption chillers or
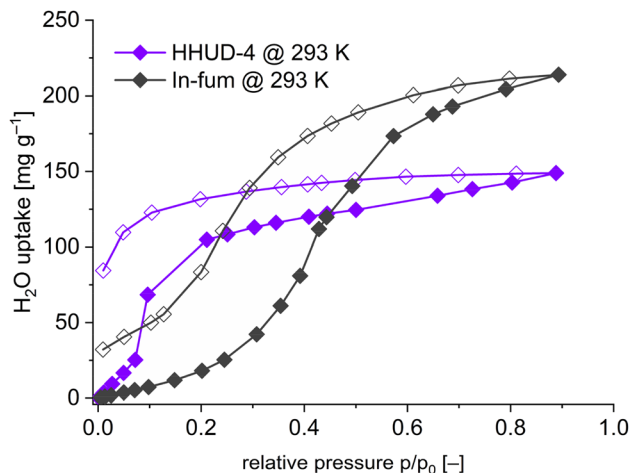
Fig. 13 Water vapor sorption isotherms for HHUD-4 and In-fum at 293 K (filled symbols for adsorption, empty symbols for desorption).

adsorption heat pumps.[18,25,30] For a good performance the uptake step should be in a p/p_0 range of 0.1 to 0.2 with a steep step and small hysteresis.[18]

Neither HHUD-4 nor In-fum fulfill these requirements as both MOFs show a very wide hysteresis in a water vapor sorption experiment at 293 K (Fig. 13). Similar to other reports in the literature the exchange of the fumarate linker through the acetylenedicarboxylate linker leads to an increased hydrophilicity of the MOF with a noticeable earlier and more sudden step in uptake at a relative pressure p/p_0 of about 0.3–0.6 for In-fum and a p/p_0 of about 0.05–0.1 for HHUD-4.[5] Yet, N_2 sorption experiments and PXRD measurements after the vapor sorption experiment (Fig. S18 and S22, ESI†) show the concomitant decomposition of HHUD-4.

Conclusions

The synthesis of the new indium acetylenedicarboxylate MOF HHUD-4 could be achieved through the reaction of indium nitrate with acetylenedicarboxylic acid. Instead of the expected *trans*-μ-OH connection of the {MO_6} octahedra with linear linkers (MIL-53 type), HHUD-4 shows for the first time *cis*-μ-OH connected polyhedra that have so far only been observed for V-shaped dicarboxylate linkers with opening angles of ~120°. With the C≡C-triple bond in the linker HHUD-4 shows high uptake capacities for CO_2 and H_2 surpassing also other adc-based MOFs and the MIL-53 analogous In-fum. Additionally, a high isosteric heat of adsorption at zero coverage for H_2 and CH_4 has been calculated for HHUD-4. For volatile organic compounds such as benzene, cyclohexane and *n*-hexane both HHUD-4 and In-fum show steep uptake steps at low relative pressures and high IAST selectivities for benzene/cyclohexane mixtures underscoring the positive role of C–C multiple bonds for benzene selectivity. There appears to be an intricate balance between *cis*-μ-OH and *trans*-μ-OH connectivity and the concomitant helical and straight {MO_6} chains in [M

(μ-OH)(linker)] MOFs for M = Al, Ga, In. One may envision that the difference between the *cis*-μ-OH/helical and *trans*-μ-OH/straight structures does not only depend on V-shaped *vs.* linear linkers but also on the synthesis conditions. That is, for HHUD-4 with the linear linker and its CAU-10-H topology there may also be a polymorph of the *trans*-μ-OH/straight MIL-53 topology. On the other hand, for Al-fum and MIL-53 there could also be polymorphs with the CAU-10-H *cis*-μ-OH/helical topology.

Author contributions

Conceptualization, C. J. (Christoph Janiak) and D. W.; methodology, D. W.; validation, D. W.; formal analysis, D. W., C. J. (Christian Jansen), T. J. M. M. N.; investigation, D. W., S. Y., A. S., C. J. (Christian Jansen), and R. O.; resources, C. J. (Christoph Janiak); data curation, D. W.; writing – original draft, D. W.; writing – review & editing, C. J. (Christoph Janiak); visualization, D. W. and C. J. (Christoph Janiak); supervision, C. J. (Christoph Janiak); project administration, C. J. (Christoph Janiak); funding acquisition, C. J. (Christoph Janiak). All authors have read and agreed to the published version of the manuscript.

Conflicts of interest

There are no conflicts to declare.

Acknowledgements

Notes and references

1 M. Safaei, M. M. Foroughi, N. Ebrahimpoor, S. Jahani, A. Omidi and M. Khatami, *TrAC, Trends Anal. Chem.*, 2019, **118**, 401.

2 C. Janiak and J. K. Vieth, *New J. Chem.*, 2010, **34**, 2366.

3 N. Stock and S. Biswas, *Chem. Rev.*, 2012, **112**, 933.

4 T. J. Matemb Ma Ntep, V. K. Gramm, U. Ruschewitz and C. Janiak, *Chem. Commun.*, 2022, **58**, 8900.

5 T. J. Matemb Ma Ntep, H. Reinsch, B. Moll, E. Hastürk, S. Gökpinar, H. Breitzke, C. Schlüsener, L. Schmolke, G. Buntkowsky and C. Janiak, *Chem. – Eur. J.*, 2018, **24**, 14048.

6 T. J. Matemb Ma Ntep, H. Reinsch, C. Schlüsener, A. Goldman, H. Breitzke, B. Moll, L. Schmolke, G. Buntkowsky and C. Janiak, *Inorg. Chem.*, 2019, **58**, 10965.

7 T. J. Matemb Ma Ntep, H. Reinsch, J. Liang and C. Janiak, *Dalton Trans.*, 2019, **48**, 15849.

8 E. Bandrowski, *Ber. Dtsch. Chem. Ges.*, 1879, **12**, 2212.

9 J. Kim, B. Chen, T. M. Reineke, H. Li, M. Eddaoudi, D. B. Moler, M. O'Keeffe and O. M. Yaghi, *J. Am. Chem. Soc.*, 2001, **123**, 8239.

10 A. Michaelides and S. Skoulika, *Cryst. Growth Des.*, 2005, **5**, 529.

11 V. K. Gramm, A. Schuy, M. Suta, C. Wickleder, C. Sternemann and U. Ruschewitz, *Z. Anorg. Allg. Chem.*, 2018, **644**, 127.

12 D. J. Tranchemontagne, J. R. Hunt and O. M. Yaghi, *Tetrahedron*, 2008, **64**, 8553.

13 F. Hohn, I. Pantenburg and U. Ruschwitz, *Chem. – Eur. J.*, 2002, **8**, 4536.

14 V. K. Gramm, D. Smets, I. Grzesiak, T. Block, R. Pöttgen, M. Suta, C. Wickleder, T. Lorenz and U. Ruschewitz, *Chem. – Eur. J.*, 2020, **26**, 2726.

15 HHUD stands for Heinrich-Heine-University Düsseldorf. HHUD-1 and -2 were reported without the "D" as HHU-1 and HHU-2 in ref. 5–7.

16 Y. Wang, S. Yuan, Z. Hu, T. Kundu, J. Zhang, S. B. Peh, Y. Cheng, J. Dong, D. Yuan, H.-C. Zhou and D. Zhao, *ACS Sustainable Chem. Eng.*, 2019, **7**, 7118.

17 A. Airi, C. Atzori, F. Bonino, A. Damin, S. Øien-Ødegaard, E. Aunan and S. Bordiga, *Dalton Trans.*, 2020, **49**, 12.

18 D. Fröhlich, E. Pantatosaki, P. D. Kolokathis, K. Markey, H. Reinsch, M. Baumgartner, M. A. van der Veen, D. E. de Vos, N. Stock, G. K. Papadopoulos, S. K. Henninger and C. Janiak, *J. Mater. Chem. A*, 2016, **4**, 11859.

19 T. Loiseau, C. Serre, C. Huguenard, G. Fink, F. Taulelle, M. Henry, T. Bataille and G. Férey, *Chem. – Eur. J.*, 2004, **10**, 1373.

20 Y. Zhang, B. E. G. Lucier, S. M. McKenzie, M. Arhangelskis, A. J. Morris, T. Friščić, J. W. Reid, V. V. Terskikh, M. Chen and Y. Huang, *ACS Appl. Mater. Interfaces*, 2018, **10**, 28582.

21 C. Serre, F. Millange, C. Thouvenot, M. Noguès, G. Marsolier, D. Louër and G. Férey, *J. Am. Chem. Soc.*, 2002, **124**, 13519.

22 F. Millange, N. Guillou, R. I. Walton, J.-M. Grenèche, I. Margiolaki and G. Férey, *Chem. Commun.*, 2008, **39**, 4732.

23 M. Wahiduzzaman, D. Lenzen, G. Maurin, N. Stock and M. T. Wharmby, *Eur. J. Inorg. Chem.*, 2018, 3626.

24 H. Reinsch, M. A. van der Veen, B. Gil, B. Marszalek, T. Verbiest, D. de Vos and N. Stock, *Chem. Mater.*, 2013, **25**, 17.

25 D. Lenzen, J. Zhao, S.-J. Ernst, M. Wahiduzzaman, A. Ken Inge, D. Fröhlich, H. Xu, H.-J. Bart, C. Janiak, S. Henninger, G. Maurin, X. Zou and N. Stock, *Nat. Commun.*, 2019, **10**, 3025.

26 T. Loiseau, C. Serre, C. Huguenard, G. Fink, F. Taulelle, M. Henry, T. Bataille and G. Férey, *Chem. – Eur. J.*, 2004, **10**, 1373.

27 M. Ghanbarian, S. Zeinali and A. Mostafavi, *Sens. Actuators, B*, 2018, **267**, 381.

28 V. Finsy, C. E. A. Kirschhock, G. Vedts, M. Maes, L. Alaerts, D. E. de Vos, G. V. Baron and J. F. M. Denayer, *Chem. – Eur. J.*, 2009, **15**, 7724.

29 M. Yousefzadeh Borzehandani, E. Abdulmalek, M. B. Abdul Rahman and M. A. Mohammad Latif, *J. Porous Mater.*, 2021, **28**, 579.

30 F. Jeremias, D. Fröhlich, C. Janiak and S. K. Henninger, *RSC Adv.*, 2014, **4**, 24073.

31 C. Jansen, N. Tannert, D. Lenzen, M. Bengsch, S. Millan, A. Goldman, D. N. Jordan, L. Sondermann, N. Stock and C. Janiak, *Z. Anorg. Allg. Chem.*, 2022, **648**, e202200170.

32 C. F. Macrae, I. Sovago, S. J. Cottrell, P. T. A. Galek, P. McCabe, E. Pidcock, M. Platings, G. P. Shields, J. S. Stevens, M. Towler and P. A. Wood, *J. Appl. Crystallogr.*, 2020, **53**, 226.

33 *APEX2, data collection program for the CCD area-detector system, Version 2.1-0*, Bruker Analytical X-ray Systems, Madison (WI), USA, 1997–2014.

34 *SAINT, data reduction and frame integration program for the CCD area-detector system*, Bruker Analytical X-ray Systems, Madison (WI), USA, 1997–2014.

35 G. M. Sheldrick, *SADABS: Area-Detector Absorption Correction*, University of Göttingen, Göttingen, Germany, 1996.

36 G. M. Sheldrick, *Acta Crystallogr., Sect. C: Struct. Chem.*, 2015, **71**, 3.

37 G. M. Sheldrick, *Acta Crystallogr., Sect. A: Found. Crystallogr.*, 2008, **64**, 112.

38 A. L. Spek, *PLATON – A Multipurpose Crystallographic Tool*, Utrecht University, Utrecht, The Netherlands, 2008; L. J. Farrugia, *Windows implementation, Version 270519*, University of Glasgow, Scotland, 2019.

39 A. Spek, *Acta Crystallogr., Sect. D: Biol. Crystallogr.*, 2009, **65**, 148.

40 K. Brandenburg, *Diamond (Version 4.5), Crystal and Molecular Structure Visualization*, Crystal Impact – K. Brandenburg & H. Putz Gbr, Bonn, Germany, 2009–2022.

41 https://en.wikipedia.org/wiki/Elongated_square_bipyramid, accessed November 17, 2022.

42 H. D. Flack, *Acta Crystallogr., Sect. A: Found. Crystallogr.*, 1983, **39**, 876.

43 H. D. Flack and G. Bernardinelli, *Acta Crystallogr., Sect. A: Found. Crystallogr.*, 1999, **55**, 908.

44 H. D. Flack and G. Bernardinelli, *Chirality*, 2008, **20**, 681.

45 H. D. Flack, M. Sadki, A. L. Thompson and D. J. Watkin, *Acta Crystallogr., Sect. A: Found. Crystallogr.*, 2011, **67**, 21.

46 H. D. Flack, *Helv. Chim. Acta*, 2003, **86**, 905.

47 A chiral space group needs to have an element from one of the following four pairs of enantiomorphous screw rotations: {31, 32}, {41, 43}, {61, 65}, {62, 64}. Only 22 out of the 230 space groups are chiral. A crystal structure in *P*21 is chiral but the space group itself is achiral since it does not form one member of an enantiomorphous pair.

48 F. H. Allen, O. Kennard, D. G. Watson, L. Brammer, A. G. Orpen and R. Taylor, *J. Chem. Soc., Perkin Trans. 2*, 1987, S1.

49 S. Biswas, T. Ahnfeldt and N. Stock, *Inorg. Chem.*, 2011, **50**, 9518.

50 F. Niekiel, M. Ackermann, P. Guerrier, A. Rothkirch and N. Stock, *Inorg. Chem.*, 2013, **52**, 8699.

51 C. Schlüsener, D. N. Jordan, M. Xhinovci, T. J. Matemb Ma Ntep, A. Schmitz, B. Giesen and C. Janiak, *Dalton Trans.*, 2020, **49**, 7373.

52 N. Reimer, H. Reinsch, A. K. Inge and N. Stock, *Inorg. Chem.*, 2015, **54**, 492.

53 V. A. Blatov, A. P. Shevchenko and D. M. Proserpio, *Cryst. Growth Des.*, 2014, **14**, 3576.

54 E. V. Alexandrov, V. A. Blatov, A. V. Kochetkov and D. M. Proserpio, *CrystEngComm*, 2011, **13**, 3947.

55 E. V. Alexandrov, A. P. Shevchenko and V. A. Blatov, *Cryst. Growth Des.*, 2019, **19**, 2604.

56 V. A. Blatov and D. M. Proserpio, *Acta Crystallogr., Sect. A: Found. Crystallogr.*, 2009, **A65**, 202.

57 P. Brandt, S.-H. Xing, J. Liang, G. Kurt, A. Nuhnen, O. Weingart and C. Janiak, *ACS Appl. Mater. Interfaces*, 2021, **13**, 29137.

58 D. Damasceno Borges, P. Normand, A. Permiakova, R. Babarao, N. Heymans, D. S. Galvao, C. Serre, G. de Weireld and G. Maurin, *J. Phys. Chem. C*, 2017, **121**, 26822.

59 J. Pei, H.-M. Wen, X.-W. Gu, Q.-L. Qian, Y. Yang, Y. Cui, B. Li, B. Chen and G. Qian, *Angew. Chem., Int. Ed.*, 2021, **60**, 25068.

60 B. C. Camacho, R. P. Ribeiro, I. A. Esteves and J. P. Mota, *Sep. Purif. Technol.*, 2015, **141**, 150.

61 D. Shade, B. Marszalek and K. S. Walton, *Adsorption*, 2021, **27**, 227.

62 Z. Huang, P. Hu, J. Liu, F. Shen, Y. Zhang, K. Chai, Y. Ying, C. Kang, Z. Zhang and H. Ji, *Sep. Purif. Technol.*, 2022, **286**, 120446.

63 3P INSTRUMENTS, *3P sim, Version 1.1.0.7, Simulation and Evaluation Tool for mixSorb*, 3P INSTRUMENTS, 2018.

64 T. J. Matemb Ma Ntep, W. Wu, H. Breitzke, C. Schlüsener, B. Moll, L. Schmolke, G. Buntkowsky and C. Janiak, *Aust. J. Chem.*, 2019, **72**, 835.

65 W. Fan, Y. Ying, S. B. Peh, H. Yuan, Z. Yang, Y. Di Yuan, D. Shi, X. Yu, C. Kang and D. Zhao, *J. Am. Chem. Soc.*, 2021, **143**, 17716.

66 S. Kavak, H. M. Polat, H. Kulak, S. Keskin and A. Uzun, *Chem. – Asian J.*, 2019, **14**, 3655.

67 Y. E. Cheon and M. P. Suh, *Chem. Commun.*, 2009, 2296.

68 W. Zhou, H. Wu and T. Yildirim, *J. Am. Chem. Soc.*, 2008, **130**, 15268.

69 B. Chen, X. Zhao, A. Putkham, K. Hong, E. B. Lobkovsky, E. J. Hurtado, A. J. Fletcher and K. M. Thomas, *J. Am. Chem. Soc.*, 2008, **130**, 6411.

70 O. K. Farha, C. E. Wilmer, I. Eryazici, B. G. Hauser, P. A. Parilla, K. O'Neill, A. A. Sarjeant, S. T. Nguyen, R. Q. Snurr and J. T. Hupp, *J. Am. Chem. Soc.*, 2012, **134**, 9860.

71 E. Barea, C. Montoro and J. A. R. Navarro, *Chem. Soc. Rev.*, 2014, **43**, 5419.

72 S. Mukherjee, A. V. Desai and S. K. Ghosh, *Coord. Chem. Rev.*, 2018, **367**, 82.

73 C. Jansen, N. Assahub, A. Spieß, J. Liang, A. Schmitz, S. Xing, S. Gökpinar and C. Janiak, *Nanomaterials*, 2022, **12**, 3614.

74 T. He, X.-J. Kong, Z.-X. Bian, Y.-Z. Zhang, G.-R. Si, L.-H. Xie, X.-Q. Wu, H. Huang, Z. Chang, X.-H. Bu, M. J. Zaworotko, Z.-R. Nie and J.-R. Li, *Nat. Mater.*, 2022, **21**, 689.

75 L.-H. Xie, X.-M. Liu, T. He and J.-R. Li, *Chem*, 2018, **4**, 1911.

76 V. K. Saini and J. Pires, *J. Environ. Sci.*, 2017, **55**, 321.

77 W. J. Krasavage, J. L. O'Donoghue, G. D. DiVincenzo and C. J. Terhaar, *Toxicol. Appl. Pharmacol.*, 1980, **52**, 433.

78 L. K. Macreadie, E. J. Mensforth, R. Babarao, K. Konstas, S. G. Telfer, C. M. Doherty, J. Tsanaktsidis, S. R. Batten and M. R. Hill, *J. Am. Chem. Soc.*, 2019, **141**, 3828.

79 Y. Xiao, A. N. Hong, Y. Chen, H. Yang, Y. Wang, X. Bu and P. Feng, *Small*, 2022, e2205119, DOI: **10.1002/smll.202205119**, early view.

80 S. Mukherjee, D. Sensharma, O. T. Qazvini, S. Dutta, L. K. Macreadie, S. K. Ghosh and R. Babarao, *Coord. Chem. Rev.*, 2021, **437**, 213852.

81 X. Lin, A. J. Blake, C. Wilson, X. Z. Sun, N. R. Champness, M. W. George, P. Hubberstey, R. Mokaya and M. Schröder, *J. Am. Chem. Soc.*, 2006, **128**, 10745.

82 V. K. Saini and J. Pires, *J. Environ. Sci.*, 2017, **55**, 321.

83 C. E. Webster, R. S. Drago and M. C. Zerner, *J. Am. Chem. Soc.*, 1998, **120**, 5509.

84 R. T. Yang, *Adsorbents Fundamentals and Applications*, John Wiley & Sons, Inc., Hoboken, New Jersey, 2003.